

Comprehensive performance of a ball-milled $La_{0.5}Pr_{0.5}Fe_{11.4}Si_{1.6}B_{0.2}H_y$/Al magnetocaloric composite

Jiao-Hong Huang(黄焦宏), Ying-De Zhang(张英德), Nai-Kun Sun(孙乃坤), Yang Zhang(张扬), Xin-Guo Zhao(赵新国), and Zhi-Dong Zhang(张志东)

Citation: Chin. Phys. B, 2022, 31 (**4**): 047503. DOI: 10.1088/1674-1056/ac280b
Journal homepage: http://cpb.iphy.ac.cn; http://iopscience.iop.org/cpb

What follows is a list of articles you may be interested in

High permeability and bimodal resonance structure of flaky soft magnetic composite materials

Xi Liu(刘曦), Peng Wu(吴鹏), Peng Wang(王鹏), Tao Wang(王涛), Liang Qiao(乔亮), Fa-Shen Li(李发伸)
Chin. Phys. B, 2020, 29 (**7**): 077506. DOI: 10.1088/1674-1056/ab8c3b

Modeling of the loading path dependent magnetomechanical behavior of Galfenol alloy

Hui Jiang(江慧), Jie Zhu(朱洁)
Chin. Phys. B, 2017, 26 (**3**): 037503. DOI: 10.1088/1674-1056/26/3/037503

Evolution of structure and magnetic properties in $PrCo_5$ magnet for high energy ball milling in ethanol

Li Zhu-Bai, Lan Jian-Ting, Zhang Xue-Feng, Liu Yan-Li, Li Yong-Feng
Chin. Phys. B, 2015, 24 (**8**): 087501. DOI: 10.1088/1674-1056/24/8/087501

Phase transitions and magnetocaloric effects in intermetallic compounds MnFe*X* (*X*=P, As, Si, Ge)

O. Tegus, Bao Li-Hong, Song Lin
Chin. Phys. B, 2013, 22 (**3**): 037506. DOI: 10.1088/1674-1056/22/3/037506

Magnetocaloric effects in $Mn_{1.35}Fe_{0.65}P_{1-x}Si_x$ compounds

Geng Yao-Xiang,Tegus O,Bi Li-Ge
Chin. Phys. B, 2012, 21 (**3**): 037504. DOI: 10.1088/1674-1056/21/3/037504

Comprehensive performance of a ball-milled $La_{0.5}Pr_{0.5}Fe_{11.4}Si_{1.6}B_{0.2}H_y$/Al magnetocaloric composite

Jiao-Hong Huang(黄焦宏)[1], Ying-De Zhang(张英德)[1], Nai-Kun Sun(孙乃坤)[2,†], Yang Zhang(张扬)[2], Xin-Guo Zhao(赵新国)[3,‡], and Zhi-Dong Zhang(张志东)[3]

[1] *State Key Laboratory of Baiyunobo Rare Earth Resource Researches and Comprehensive Utilization, Baotou Research Institute of Rare Earths, Baotou* 014030, *China*

[2] *School of Science, Shenyang Ligong University, Shenyang* 110159, *China*

[3] *Shenyang National Laboratory for Materials Science, Institute of Metal Research, Chinese Academy of Sciences, Shenyang* 110016, *China*

(Received 15 August 2021; revised manuscript received 13 September 2021; accepted manuscript online 18 September 2021)

Due to the hydrogen embrittlement effect, La(Fe,Si)$_{13}$-based hydrides can only exist in powder form, which limits their practical application. In this work, ductile and thermally conductive Al metal was homogeneously mixed with $La_{0.5}Pr_{0.5}Fe_{11.4}Si_{1.6}B_{0.2}$ using the ball milling method. Then hydrogenation and compactness shaping of the magnetocaloric composites were performed in one step via a sintering process under high hydrogen pressure. As the Al content reached 9 wt.%, the $La_{0.5}Pr_{0.5}Fe_{11.4}Si_{1.6}B_{0.2}H_y$/Al composite showed the mechanical behavior of a ductile material with a yield strength of $\sim$ 44 MPa and an ultimate strength of 269 MPa accompanied by a pronounced improvement in thermal conductivity. Due to the ease of formation of Fe–Al–Si phases and the several micron and submicron sizes of the composite particles caused by ball milling process, the magnetic entropy change of the composites was substantially reduced to $\sim$ 1.2 J/kg·K–1.5 J/kg·K at 0 T–1.5 T.

Keywords: ball milling, mechanical behavior, room-temperature magnetic refrigeration, La(Fe,Si)$_{13}$

PACS: 75.30.Sg, 62.20.–x **DOI:** 10.1088/1674-1056/ac280b

1. Introduction

La(Fe,Si)$_{13}$-based hydrides have demonstrated a great potential for applications in room-temperature magnetic refrigeration by virtue of their large magnetic entropy change, abundant constituent elements and cascading of magnetic transition temperature across the near room-temperature range by Mn substitution or adjustment of the hydrogen content.[1,2] However, due to the hydrogen embrittlement effect, La(Fe,Si)$_{13}$-based hydrides can only exist in powder form, which poses a challenge for shaping these materials into bulk magnetocaloric refrigerants for various regenerator configurations. Recently, a metal-bonding approach was employed for bulk formation of La(Fe,Si)$_{13}$ hydrides and this had the simultaneous effect of enhancing the mechanical and thermal conduction properties.[3–5] Compared with other metal bonders, such as Cu, Bi, In and Sn, metal Al possesses a better comprehensive performance with a unique combination of strength and corrosion resistance, non-toxicity and low cost, and high ductility and thermal conductivity.[6] In first-order transition of giant magnetocaloric materials, substitution or addition of B could reduce the lattice volume discontinuities at the transition temperature, thereby reducing the hysteresis loss[7] and improving mechanical stability.[8]

In our previous works,[9,10] a series of La(Fe,Si)$_{13}$ bulk hydrides were prepared by sintering under high hydrogen pressure. Unfavorably, in these sintered hydrides, a large number of micropores were distributed in the main phase matrix, substantially reducing the compressive strength and thermal conductivity. Considering these aforementioned factors, in this work we employ metal Al as a bonder to produce $La_{0.5}Pr_{0.5}Fe_{11.4}Si_{1.6}B_{0.2}H_y$/Al bulk composites. Hydrogenation and compactness shaping of the magnetocaloric composites were fulfilled in one step via a high-pressure sintering process. The comprehensive performance associated with application in magnetic refrigeration was systematically explored.

2. Experiment

The parent compounds of $LaFe_{11.4}Si_{1.56}$ and $La_{0.5}Pr_{0.5}Fe_{11.4}Si_{1.6}B_{0.2}$ were prepared by melting starting materials with purity of $\geq$ 99.9 wt.% using a medium-frequency induction furnace, as described in detail in Ref. [11]. The ball milling method was employed to homogeneously mix the La(Fe,Si)$_{13}$-based compounds with metal Al according to weight ratios of 60:1, 10:1, and 5:1; the resultant composites are referred to as 1.6 wt.% Al, 9 wt.% Al, and 16.7% wt.% Al samples, respectively. The materials were sealed in a hardened steel vial in a high-purity argon atmosphere and then ball milled for 30 min. The ball-milled powders were cold-pressed into thin plates (12.6-mm diameter, 1-mm thick) and sintered for 10 min at 290 °C in a

†Corresponding author. E-mail: naikunsun@163.com
‡Corresponding author. E-mail: xgzhao@imr.ac.cn

© 2022 Chinese Physical Society and IOP Publishing Ltd

high-pressure H_2 atmosphere of 50 MPa for hydrogenation and compaction. Subsequent annealing was conducted at 200 °C for 2 h to reduce interface defects. Importantly, a high-pressure atmosphere was retained during the whole annealing and cooling process to suppress hydrogen desorption.

X-ray diffraction (XRD) analysis was carried out using Cu-K_α radiation in a Rigaku D/Max-γA diffractometer. The microstructure and elemental composition of the composites were characterized by means of a FEI Quanta 200 F scanning electron microscope (SEM) equipped with an energy-dispersed x-ray (EDX) spectrometer. The compressive strain–stress curve was measured with a universal testing machine. The magnetic properties were measured with a superconducting quantum interference device magnetometer using the reciprocating sample option as the measurement mode. The adiabatic temperature changes ΔT_{ad} were directly measured using a self-made setup.[11] A laser flash thermal conductivity apparatus (LFA 457) was employed for measuring the thermal conductivity λ along the vertical direction of the sintered thin plates by directly measuring the thermal diffusivity, D, and indirectly deriving the specific capacity C_p using a representative Cu sample.

3. Results and discussion

For a good compactness effect, with the premise of ensuring stability of the 1:13 main phase, the sintering temperature should be as high as possible. To explore the optimum sintering temperature, we first sintered the ball-milled $LaFe_{11.4}Si_{1.56}$/Al composite at 500 °C for 2 h. The XRD pattern shows a strong combined reflection peak of the $Fe_3Al_{0.5}Si_{0.5}$ phase and α-Fe at $\sim 45°$ and an intermetallic phase, Fe_2Al_5, is also formed. Notably, upon hydrogenation the reflections of the cubic $NaZn_{13}$-type structure unexpectedly shift to higher angles, indicating substantial decomposition of the 1:13 main phase (Fig. 1(a)). After checking the phase constitutions of the sintered composites, the optimum sintering temperature and time were determined to be 290 °C and 10 min, respectively. Selected XRD patterns of as-prepared $La_{0.5}Pr_{0.5}Fe_{11.4}Si_{1.6}B_{0.2}H_y$/Al composites are shown in Fig. 1(b). For the 1.6 wt.% Al sample, the reflection peak of pure Al is not detected, and with increase in the Al content to 9 wt.% and 16.7 wt.%, an apparent reflection peak of pure Al is observed. Small reflection peaks were identified to correspond to θ-Al_2O_3 and $FeAl_9Si_3$, indicating that Al is easy to oxidize in the ball milling process.

Figures 2(a)–2(c) illustrate the fracture and surface morphology of the 9 wt.% Al sample. An EDX study was carried out in eight typical areas A–H for analyzing the Al distribution and phase compositions. The grey area A on the fracture surface has a small concentration of Al (2.5 at.%) and a predominant concentration of the 1:13 main phase. The elemental compositions in the dark area B are mostly Al (28 at.%) and O (71 at.%) with small concentration of Fe (0.6 at.%) and Si (0.2 at.%), indicating that this kind of grey area predominantly consists of Al_2O_3. Area C, corresponding to a single large $La_{0.5}Pr_{0.5}Fe_{11.4}Si_{1.6}B_{0.2}H_y$ particle, has the smallest Al concentration of 1.5 at.% and areas D and E contain an Al concentration of 10 at.%–15 at.%. The surface morphology in Fig. 2(c) clearly shows three typical areas, a white area F, a grey area G and a dark grey area H. The Al concentrations for areas F and G are 15 at.% and 1 at.%, respectively. Area H contains 41 at.% O and 13 at.% Al, indicating that this kind of dark grey area on the surface is mainly composed of Al_2O_3.

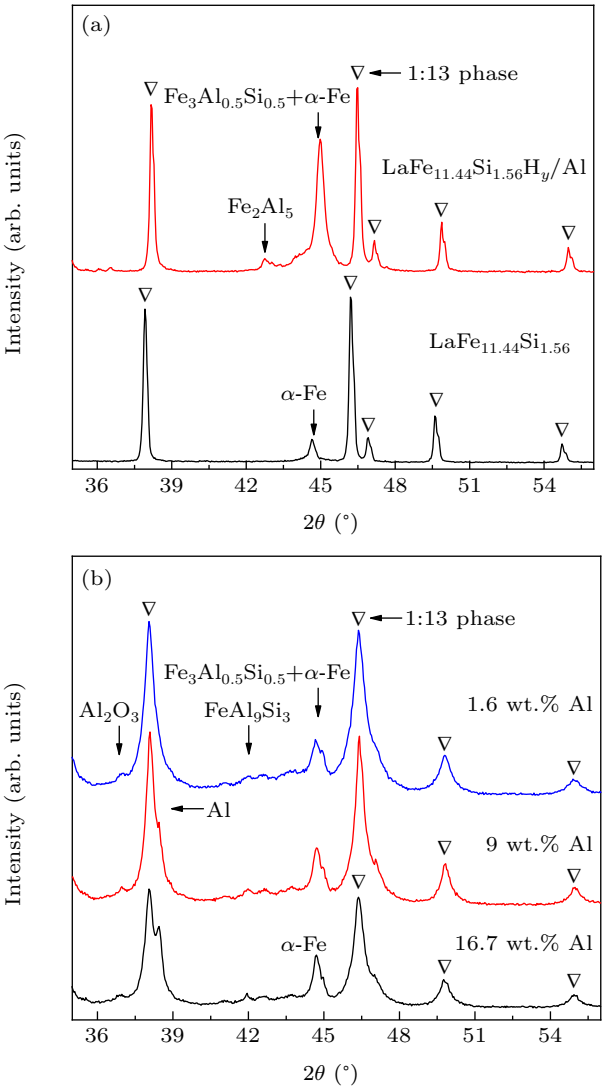


Fig. 1. Selected XRD patterns of (a) $LaFe_{11.4}Si_{1.56}$ and $LaFe_{11.4}Si_{1.56}H_y$/Al (4 wt.%) composite and (b) $La_{0.5}Pr_{0.5}Fe_{11.4}Si_{1.6}B_{0.2}H_y$/Al composites.

From the expanded view of fracture morphology (Fig. 2(b)) and surface morphology (Fig. 2(c)), we can clearly observe that the particles have a large size distribution ranging from submicron to $\sim$ 10 microns with a predominant number of particles having sizes of several microns; this can be ascribed to the ball milling process. In contrast, La(Fe,Si)$_{13}$-based bulk hydrides prepared by other methods generally have

much larger particle sizes of tens of microns.[12,13] Together, the results of XRD and EDX analyses indicate that upon ball milling, aluminum oxides fill up the gaps and pure Al, Fe–Al–Si alloys and α-Fe are distributed in the 1:13 main phase particles; these cannot be individually identified.

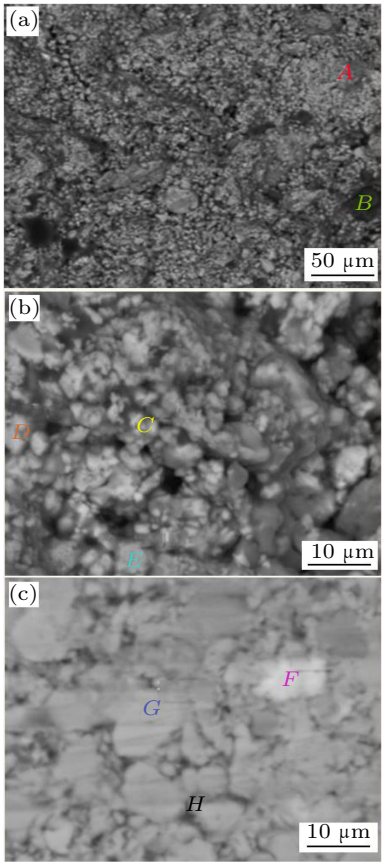


Fig. 2. SEM images of (a) and (b) fracture morphology and (c) surface morphology of $La_{0.5}Pr_{0.5}Fe_{11.4}H_y$/Al (9 wt.%).

The distribution of ductile Al bonder in the 1:13 phase matrix as well as the fact that the gaps are filled up with Al_2O_3 should remarkably enhance the mechanical and thermal conduction properties. As shown in Fig. 3, the compressive strength of 42 MPa for the 1.6 wt.% Al-bonded composite is in a similar range of magnitude to the sintered (36 MPa–46 MPa)[9] and epoxy-resin-bonded $La(Fe,Si)_{13}$ hydrides (52 MPa).[13] Moreover, these bulk hydrides prepared by different methods all show a similar shape of the stress–strain curve associated with the mechanical behavior of brittle materials. As the Al content increases to 9 wt.%, the stress–strain diagram demonstrates typical characteristic of ductile materials, with a long yielding stage beginning at the yield strength of $\sim$ 44 MPa followed by a strain hardening process. This ductile mechanical behavior has not previously been observed in $La(Fe,Si)_{13}$ composites bonded by other ductile metals such as In,[4] Sn,[14] and Bi,[15] and is also absent in a $LaFe_{11}Co_{0.8}Si_{1.2}$/10 wt.% Al composite prepared by the hot-pressing method.[6] The present 16.7 wt.% Al sample demonstrates an ultimate compressive strength of 388 MPa, much higher than the values for the hot-pressed $LaFe_{11}Co_{0.8}Si_{1.2}$/10 wt.% Al composite (186 MPa) and 20 wt.% Cu-bonded $La_{0.8}Ce_{0.2}(Fe_{0.95}Co_{0.05})_{11.8}Si_{1.2}$ (248 MPa).[12] Consolidated alumina powder bodies show particle size-dependent plastic to brittle transition due to the fact that, for a given applied pressure, larger forces exist between larger particles as a result of the smaller number of contacts per unit volume.[16] Smaller wood particle sizes correspond to a higher ultimate compression strength in wood-based composites, as the larger surface area for smaller particles could act as an adhesive factor in the composite system and lead to a more efficient stress transfer.[17] It has been observed in SiC particle-reinforced Al–Cu alloy composites that a small particle size of several microns and uniform distribution of the reinforcing phase corresponded to the highest yield strength and ultimate tensile strength.[18] According to these previous results, the high compressive strength and mechanical behavior of ductile materials in the present $La_{0.5}Pr_{0.5}Fe_{11.4}Si_{1.6}B_{0.2}H_y$/Al composite can be ascribed to the fact that the ball milling results in Al particles being distributed in the whole matrix as well as the small particle size of the composites.

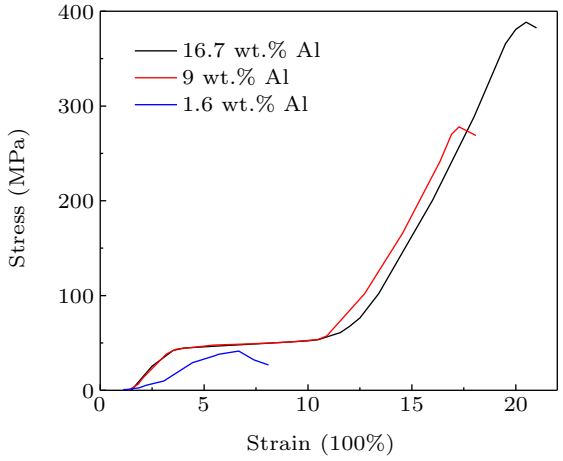


Fig. 3. Compressive stress–strain curves for $La_{0.5}Pr_{0.5}Fe_{11.4}Si_{1.6}B_{0.2}H_y$/Al composites.

Next, we evaluate the magnetocaloric properties of the Al-bonded composites. The thermomagnetic curves of the composites in a field of 0.01 T are shown in Fig. 4(a). The Curie temperature, T_C, defined as the minimum of the dM/dT versus T curves, is $\sim$ 320 K for the 1.6 wt.% Al sample and $\sim$ 324 K for the two samples with higher Al contents. The temperature dependence of $\Delta S_m(T,B)$ calculated from the isothermal magnetization data (Figs. 4(b)–4(d)) using the Maxwell relationship is shown in Fig. 5(a). The maximum value of ΔS_m of the $La_{0.5}Pr_{0.5}Fe_{11.4}Si_{1.6}B_{0.2}H_y$/Al composites is reduced by approximately fivefold to $\sim$ 1.2 J/kg·K–1.5 J/kg·K for a magnetic field change of 1.5 T compared with

(La,Pr)(Fe,Si)$_{13}$-based hydrides.[19–21] This can be mainly ascribed to the small particle size[22] due to the ball milling process as well as the existence of non-magnetocaloric phases of Fe–Al–Si alloys and pure Al. The directly measured adiabatic temperature change ΔT_{ad} is represented in Fig. 5(b). The peak value of ΔT_{ad} for a field change of 1.5 T is 0.54 K at 322 K, 0.48 K at 330 K and 0.45 K at 325 K for the 1.6 wt.% Al, 9 wt.% Al, and 16.7 wt.% Al composites, respectively.

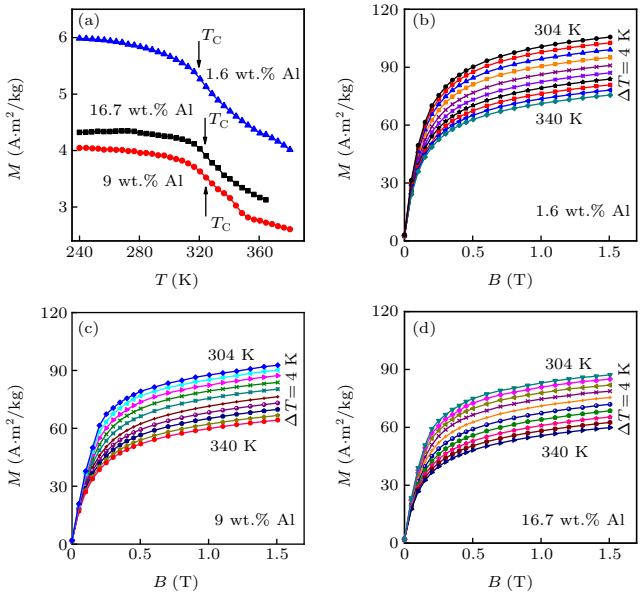


Fig. 4. (a) Thermomagnetic magnetization curves and (b)–(d) isothermal magnetization curves of $La_{0.5}Pr_{0.5}Fe_{11.4}Si_{1.6}B_{0.2}H_y$/Al composites.

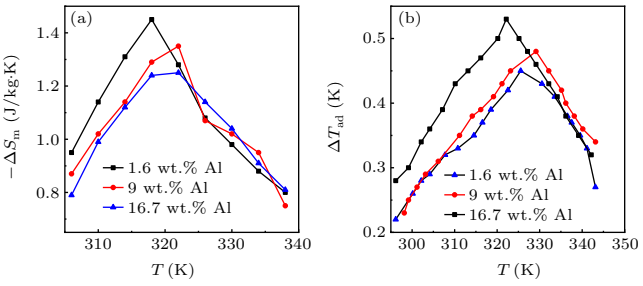


Fig. 5. The temperature dependence of ΔS_m (a) and ΔT_{ad} (b) for $La_{0.5}Pr_{0.5}Fe_{11.4}Si_{1.6}B_{0.2}H_y$/Al composites.

High thermal conductivity of magnetocaloric materials is desirable for application in a refrigerant device in order to afford efficient heat transfer to the heat exchange fluid. Hot-pressing or sintering cannot ensure uniform distribution of thermal conductive metal particles in La(Fe,Si)$_{13}$ hydride matrices, making the λ values lower than expected, such as 2 W/K·m–3 W/K·m for the 4 wt.% Cu bonded,[3] 5 W/K·m for the 15 wt.% silver-epoxy bonded[23] and 6.8 W/K·m for the 25 wt.% Sn bonded[14] composites. Figure 6 represents the thermal conductivity of $La_{0.5}Pr_{0.5}Fe_{11.4}Si_{1.6}B_{0.2}H_y$/Al composites in the temperature range covering the phase transition temperature. The λ values in the paramagnetic state are generally a little higher than those in the ferromagnetic state. The room-temperature λ in the cross-plane direction of the sintered plates is 1.9 W/K·m, 3.7 W/K·m, and 11.1 W/K·m for the 1.6 wt.%, 9 wt.%, and 16.7 wt.% Albonded composites, respectively, indicating that metal Al has a similar effect on thermal conductive improvement of La(Fe,Si)$_{13}$ hydrides to metal In.[4] A plastically deformed La(Fe,Si)$_{13}$ plate demonstrated significant anisotropic thermal conductivity in cross-plane and in-plane directions mainly due to the in-plane elongation of α-Fe and the 1:13 phase grains caused by open-die forging.[24] The present composites prepared by ball milling and short-duration sintering do not exhibit an apparent anisotropic microstructure, so we expect no substantial directional difference in λ for the Al-bonded La–Fe–Si composites.

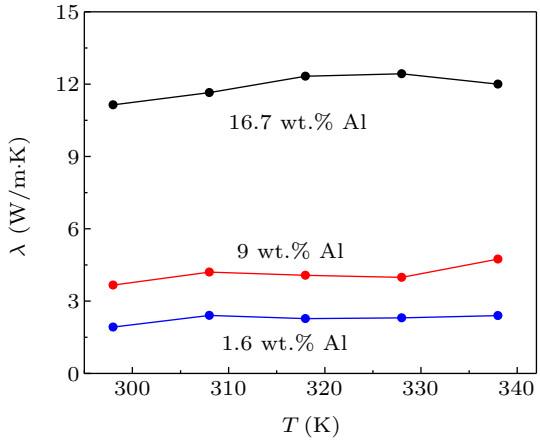


Fig. 6. Thermal conductivity of $La_{0.5}Pr_{0.5}Fe_{11.4}Si_{1.6}B_{0.2}H_y$/Al composites at temperatures across the phase transition temperature.

4. Conclusion

We have developed a novel route for the fabrication of La(Fe,Si)$_{13}$ hydride-based bulk materials via ball-milling mixing and sintering at high hydrogen pressure. Upon incorporating 9 wt.%–16.7 wt.% Al, the as-prepared $La_{0.5}Pr_{0.5}Fe_{11.4}Si_{1.6}B_{0.2}H_y$/Al composites demonstrate the mechanical behavior of ductile materials with a yield strength of 44 MPa and ultimate strength of 269 MPa–388 MPa. The 16.7 wt.% Al-bonded composite has a high thermal conductivity of 11.1 W/K·m, which is comparable to the effect of metal In bonding. The ball milling process facilitates the homogeneous distribution of metal Al in the matrix, but simultaneously reduces the particle size even to the submicron range, leading to a substantial decrease in the magnetocaloric effect.

Acknowledgments

Project supported by the Open Research Project of State Key Laboratory of Baiyunobo Rare Earth Resource Researches and Comprehensive Utilization and the National Natural Science Foundation of China (Grant Nos. 51771197 and 52171187).

References

[1] Vieira B P, Bez H N, Kuepferling M, Rosa M A, Schafer D, Cid C C P, Vieyra H A, Basso V, Lozano J A and Barbosa J R 2021 *Appl. Therm. Eng.* **183** 116185

[2] Zhang H, Gimaev R, Kovalev B, Kamilov K, Zverev V and Tishin A 2019 *Physica B* **558** 65

[3] Lia Y Q, Wu Q C, Shen F R, Zhou H B, Hu F X, Wang J, Sun J R and Shen B G 2019 *Intermetallics* **106** 124

[4] Wang Y X, Zhang H, Liu E K, Zhong X C, Tao K, Wu M L, Xing C F, Xiao Y N, Liu J and Long Y 2018 *Adv. Electron. Mater.* **4** 1700636

[5] Radulov I A, Karpenkov D Y, Skokov K P, Karpenkov A Y, Braun T, Brabänder V, Gottschall T, Pabst M, Stoll B and Gutfleisch O 2017 *Acta Mater.* **127** 389

[6] Zhang M X, Ouyang Y, Zhang Y F and Liu J 2020 *J. Alloys Compd.* **823** 153846

[7] Guillou F, Yibole H, van Dijk N H, Zhang L, Hardy V and Bruck E 2014 *J. Alloys Compd.* **617** 569

[8] Zhang H, Long Y, Cao Q, Mudryk Y, Zou M, Gschneidner K A and Pecharsky V K 2010 *J. Magn. Magn. Mater.* **322** 1710

[9] Sun N K, Zhang Y, Zhao X G, Guo J, Cheng J, Huang J H and Zhang Z D 2020 *J. Magn. Magn. Mater.* **495** 165889

[10] Sun N K, Zhao X G, Song Y W, Liu R Q, Guo J, Zhang Y, Huang J H and Zhang Z D 2021 *J. Magn. Magn. Mater.* **525** 167685

[11] Xia W, Huang J H, Sun N K, Liu C L, Ou Z Q and Song L 2015 *J. Alloys Compd.* **635** 124

[12] Peng D R, Zhong X C, Huang J H, Zhang H, Huang Y L, Dong X T, Jiao D L, Liu Z W and Ramanujan R V 2018 *MRS Commun.* **8** 1216

[13] Zhang H, Sun Y J, Niu E, Hu F X, Sun J R and Shen B G 2014 *Appl. Phys. Lett.* **104** 062407

[14] Zhang H, Liu J, Zhang M X, Shao Y Y, Li Y and Yan A 2016 *Scripta Mater.* **120** 58

[15] Liu Z G, Wu Q M, Sun N K, Ding Z and Li L W 2018 *Materials* **11** 943

[16] Franks G V and Lange F F 1999 *Colloids and Surfaces A: Physicochem. Eng. Aspects* **146** 5

[17] Jaya H, Omar M F, Akil H M, Ahmad Z A and Zulkepli N N 2016 *BioResources* **11** 6489

[18] Wang Z W, Song M, Sun C and He Y H 2011 *Mater. Sci. Eng. A* **528** 1131

[19] Sun N K, Ren Z X, Guo, Si P Z and Sun M Z 2017 *AIP Adv.* **7** 056419

[20] Xu L, Zhao J L, Yang J J, Zhang H G, Liu D M, Yue M and Jang Y J 2017 *Chin. Phys. B* **26** 067502

[21] Liu Q, Tong M, Zhao X G, Sun N K, Xiao X F, Guo J, Liu W and Zhang Z D 2021 *Chin. Phys. B* **30** 087502

[22] Hu F X, Chen L, Wang J, Bao L F, Sun J R and Shen B G 2012 *Appl. Phys. Lett.* **100** 072403

[23] Radulov L A, Skokov K P, Karpenkov D Y, Braun T and Gutfleisch O 2015 *J. Magn. Magn. Mater.* **396** 228

[24] Ouyang Y, Zhang M X, Yan A, Wang W, Guillou F and Liu J 2020 *Acta Mater.* **187** 1